ACS SENSORS

Article

Cite This: ACS Sens. 2018, 3, 1750−1755

pubs.acs.org/acssensors

DNA Melting Analysis with Optofluidic Lasers Based on Fabry-Pérot Microcavity

Mengdi Hou,[†,§] Xiyue Liang,[†,§] Tingting Zhang,[†] Chengyu Qiu,[†] Jingdong Chen,[†] Shaoding Liu,[†] Wenjie Wang,[*,†] and Xudong Fan[*,‡]

[†]Key Lab of Advanced Transducers and Intelligent Control System of Ministry of Education, Taiyuan University of Technology, 79 Yingze Street, Taiyuan 030024, P. R. China

[‡]Department of Biomedical Engineering, University of Michigan, 1101 Beal Avenue, Ann Arbor, Michigan 48109, United States

Supporting Information

ABSTRACT: We conduct DNA high-resolution melting (HRM) analysis using optofluidic lasers based on a Fabry-Pérot microcavity. Compared to the fluorescence-based HRM, the laser-based HRM has advantages of higher emission intensity for better signal-to-noise ratio and sharper transition for better temperature resolution. In addition, the melting temperature can be lowered by optimizing the laser conditions such as external pump and cavity *Q*-factor. In this work, we first theoretically analyze the laser-based HRM. Then experiments are performed on three long DNA sequences as model systems, one being 99 bases and the other two being 130 bases long but with different GC contents. We show that the laser-based HRM is able to distinguish the target and the single-base mismatched DNA as long as 130 bases and with nearly 50% GC content. The dependence of laser threshold on the temperature for each DNA sample is first experimentally investigated and by optimizing the external pump, the melting temperature is reduced by more than 10 °C, compared to the fluorescence-based HRM for long DNA sequences up to 130 bases. Finally, we demonstrate an alternative method of using the laser-based HRM for rapid DNA screening that does not exist for the fluorescence-based HRM, in which laser excitation is scanned at a fixed temperature to distinguish the target and the base-mismatched DNA sequences. It is shown that the 130-bases-long DNA with nearly 50% GC content can have as much as 20% difference in the laser threshold and 40% difference in the laser output slope between the target and the single-base mismatched sequences, despite only 0.5 °C difference in their melting temperature, indicating that the laser-excitation-scanning method can also be suitable for long DNA sequences with higher GC content.

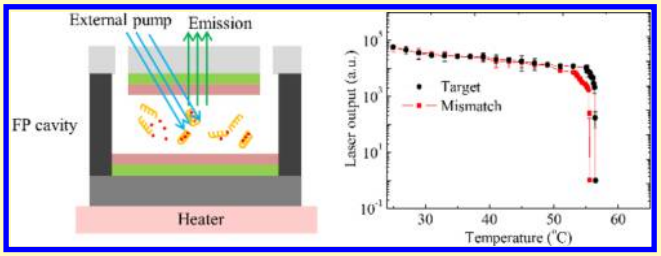

KEYWORDS: *high-resolution melting, optofluidic lasers, Fabry-Pérot microcavity, DNA analysis, intracavity detection*

As a DNA-analyzing platform, high-resolution melting (HRM) analysis is a simple, fast, and cost-effective way to analyze DNA sequences that may have mutation and methylation.[1−6] Current HRM employs fluorescence from intercalating saturation dyes as the sensing signal. It relies on the thermodynamic difference between the target and the single-base mismatched DNA to distinguish them by changing the ambient temperature. Recently, the laser-based HRM DNA analysis was proposed, which utilizes optical amplification of the signals inside a laser cavity.[7] Compared to the fluorescence-based HRM, the laser-based HRM has several advantages. First, laser signal is much stronger than fluorescence and thus provides a much higher discrimination ratio between the target and the base-mismatched DNA.[7] The melting curve of the laser-based HRM is much sharper, as it represents the phase transition between stimulated emission and spontaneous emission (i.e., fluorescence), which results in a better temperature resolution. Third, while the melting temperature of the fluorescence-based HRM (referred to as the true melting temperature), defined as the temperature where the fluorescence decreases by 50%, depends solely on the thermodynamics of a DNA sequence, the melting temperature of the laser-based HRM (referred to as the apparent melting temperature, different from the true melting temperature of the fluorescence-based HRM), defined as the temperature where the sharp phase transition occurs from stimulated laser emission to spontaneous emission, depends on not only the thermodynamics of a DNA sequence but also optical conditions of the laser such as the cavity *Q*-factor and external excitation. Thus, the melting temperature of the laser-based HRM can be adjusted arbitrarily within a certain temperature range, depending on the laser condition. Consequently, it may be possible for us to optimize the optical conditions to our benefit, such as shifting the melting temperature to a lower temperature range by using a lower external excitation and/or a lower *Q*-factor. Finally, the laser-based HRM can potentially provide another way for rapid DNA screening by scanning

Received: June 9, 2018
Accepted: August 24, 2018
Published: August 24, 2018

DOI: 10.1021/acssensors.8b00481
ACS Sens. 2018, 3, 1750−1755

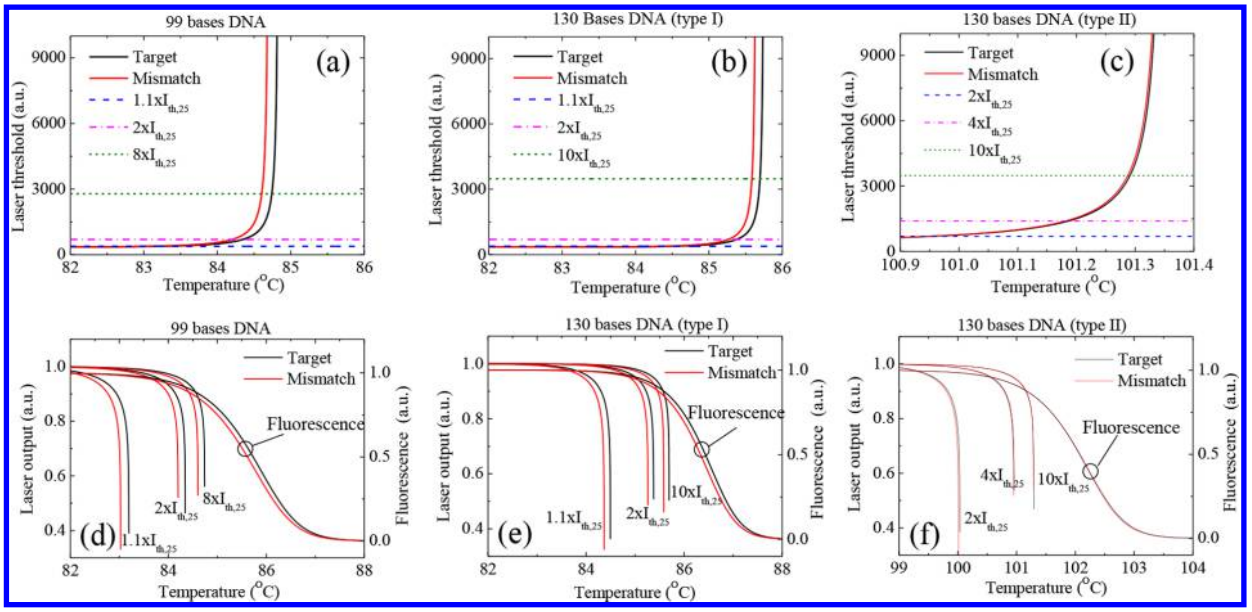

Figure 1. (a–c) Theoretically calculated laser threshold, I_{th}, as a function of temperature for 99 bases (a), type I 130 bases (b), and type II 130 bases (c) DNA sequences according to eq 1. See detailed information on DNA sequences in Table S2. The black and red solid lines represent the target and single-base mismatched DNA sequence, respectively. The horizontal lines represent different external pump intensities. $I_{th,25}$ is the laser threshold at 25 °C. The *Q*-factor of the cavity is 3×10^4 and the calculated γ is 0.78. Please refer to Table S1 for more other parameters used in the simulation. (d–f) Corresponding laser output as a function of temperature for 99 bases (d), type I 130 bases (e), and type II 130 bases (f). DNA sequences in the laser-based HRM using different external pump intensities. The corresponding fluorescence-based HRM curves are also plotted. All curves are normalized to the signal at 25 °C. The details of the melting temperature and the melting temperature difference can be found in Table S4.

laser excitation at a fixed temperature to distinguish the target and the base-mismatched DNA sequence, a unique characteristic that does not exist for the fluorescence-based HRM.

While the laser-based HRM was demonstrated using a capillary-based ring resonator as the laser cavity,[7] there are a number of areas that need improvement and further exploration. For example, though simple, the capillary based ring resonator is difficult to integrate with a temperature control system for better temperature resolution due to its circular shape and the low thermal conductivity of the glass material. In addition, it is difficult for the capillaries to form an array on a chip to achieve high-throughput HRM analysis. Finally, lowering the melting temperature by optimization of the laser conditions, such as optimization of the pumping intensity and the *Q*-value of the laser cavity, has not yet been extensively explored.

In this work, we use a Fabry-Pérot (FP) cavity on a chip as the laser cavity, which can be mass-produced and is highly compatible with a temperature control system due to its planar structure and high thermal conductivity. Thanks to the microfluidic design, the volume of DNA sample can be as low as a few nanoliters. We conduct theoretical analysis and experiments on laser-based HRM using long DNA sequences of 99 and 130 bases as model systems. The dependence of the laser threshold on the temperature is first experimentally investigated, and accordingly by optimizing pump intensity the melting temperature of the laser-based HRM can be lowered by more than 10 °C, compared to that of the fluorescence-based HRM, especially for long-bases DNA sequences, thus alleviating the issues such as solution boiling caused by high temperature. We also demonstrate a fast DNA screening method by scanning the laser excitation at a fixed and lower temperature to distinguish the target and the single-base-mismatched long DNA sequences.

THEORETICAL ANALYSIS

According to the laser theory, the laser threshold, I_{th}, is determined by[7,8]

$$I_{th} = \frac{\gamma}{\Gamma - \gamma} \tag{1}$$

where γ is the required fraction of the dye molecules in the excited state at the onset of lasing. γ is related to the laser cavity *Q*-factor and dye properties (e.g., emission and absorption cross section at lasing wavelength, dye concentration). The expression of γ and the corresponding parameters used in the simulation are listed in Table S1 in the Supporting Information. Γ is the fraction of the dyes that are intercalated in the double-stranded DNA at temperature T (i.e., $\Gamma = n_{dsDNA}/n_{total}$, where n_{total} is the total concentration of the dye. n_{dsDN}A is the concentration of the dye that binds to double-stranded DNA and should be proportional to the double-stranded DNA concentration). Only when the dyes intercalated in the double-stranded DNA do they fluoresce and participate in lasing. According to the thermodynamics, when the temperature increases, double-stranded DNA gradually melts into single-stranded DNA, accompanied by the release of intercalated dye molecules into the solution, resulting in a decreased Γ. Detailed calculation of Γ can be found in refs 7, 8. According to the laser theory, the output laser intensity, I_{laser}, is proportional to the pump intensity, I_{pump}, above the laser threshold, i.e.,

$$I_{laser} \propto \left(\frac{I_{pump}}{I_{th}} - 1 \right) \tag{2}$$

DOI: 10.1021/acssensors.8b00481
ACS Sens. 2018, 3, 1750–1755

Note that in the fluorescence-based HRM, the output fluorescence intensity is proportional to Γ, i.e.,

$$I_{\text{fluor}} \propto \Gamma \tag{3}$$

In the theoretical analysis and subsequent experiments, we use 3 pairs (target and single-base mismatched) of DNA sequences having 99 bases and 130 bases. Table S2 provides the details of those sequences. In particular, the 130 DNA sequences have two types. Type I has a lower GC contents than type II, which results in a different thermodynamics.

Figure 1a–c presents the calculated laser threshold as a function of temperature for the target and the single-base mismatched DNA of 99 bases and 130 bases (type I and type II) based on eq 1. The corresponding melting curves, i.e., the laser output as a function of temperature, are given in Figure 1d–f. Here we use Figure 1a,d as an example to discuss the laser characteristics and the melting curve. From Figure 1a it is easily seen that the laser threshold does not change much at relatively low temperature, as the melting of the double-stranded DNA does not occur. With the increased temperature, the threshold increases rapidly due to decreased Γ. When the fixed external pump, which is represented by the horizontal dashed line, is higher than the threshold, strong laser output is obtained (see Figure 1d). With the increased temperature, the threshold increases. Consequently, the laser output decreases precipitously. Once the threshold surpasses the external pump, the laser emission stops, resulting in nearly zero output. This process can be seen clearly in the melting curve in Figure 1d. The melting temperature in the laser-based HRM can be defined as the temperature at which the laser threshold surpasses the external pump and laser emission stops (due to the phase transition from stimulated emission to spontaneous emission). Figure 1a,d shows that the melting temperature depends on the external pump—a lower external pump resulting in a lower melting temperature. For example, the melting temperature is decreased by about 1.6 °C when the external pump decreases from 8 × $I_{\text{th,25}}$ (well above the laser threshold) to 1.1 × $I_{\text{th,25}}$ (just above the laser threshold). In addition, regardless of the external pump the target DNA always has a higher melting temperature than the corresponding single-base mismatched DNA due to higher affinity. Moving to longer DNA sequences that have higher affinity, the overall laser characteristics and the melting curves remain the same, except that the melting temperature shifts to a higher temperature and the melting temperature difference between the target and the single-base mismatched DNA decreases.

For comparison, Figure 1d–f also plots the corresponding fluorescence-based HRM curves and reveals three major differences between the fluorescence- and laser-based HRM. First, the laser-based HRM curve is much sharper due to the phase transition between stimulated emission and spontaneous emission, which leads to a better resolution to determine the melting temperature. Second, the laser-based HRM has a lower melting temperature. Third, the melting temperature can be adjusted by the external pump. Particularly, a lower pump results in a lower melting temperature. It is noteworthy that the melting temperature can also be lowered by using a laser cavity with a lower *Q*-factor (see Figure S1 for detailed simulation). Moving the melting temperature to a lower temperature range has a number of advantages such as ease of system design and temperature control, avoidance of solution boiling and evaporation issues at high temperature, and capability to analyze longer DNA sequences.

EXPERIMENTAL SECTION

Materials. The linearly structured target and the corresponding single-base-mismatched DNA sequence used in the experiment are 99 bases long with GC content of 22.5%, 130 bases long with GC content of 21.5% (type I), and 130 bases long with GC content of 48.5% (type II). The sequence information is given in Table S2. The DNA samples are synthesized by Sangon Biotech Company. SYTO 13 nucleic acid stain (Invitrogen, originally dissolved in DMSO with 5 mM concentration) is used as the saturation dye and is separately mixed with the target and the mismatch samples. The mixture of DNA and the saturation dye is dissolved in the buffer solution (Tris-acetate-EDTA buffer, pH = 8.3) with the final concentration of 50 μM and 500 μM for 99-bases-long DNA samples and the saturation dye, and with the final concentration of 50 μM and 650 μM for 130-bases-long DNA samples and the saturation dye.

Optical Setup. The experimental setup is illustrated in Figure 2. The FP cavity used in our experiment consists of two planar mirrors

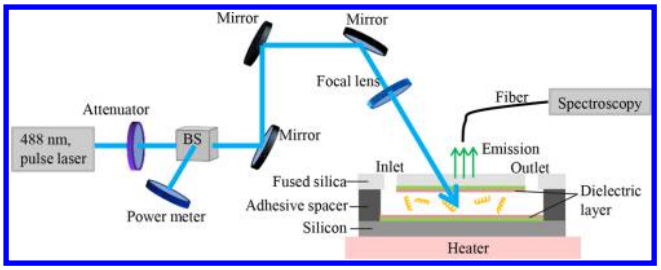

Figure 2. Schematic of the experimental setup.

(reflectivity ≥99.9% @ 540 nm) coated with 15 pairs of alternative dielectric layers SiO_2 and Ta_2O_5. The double-sided adhesive tape is cut into small stripes, which are subsequently placed on the two mirrors. The cavity length is 30 μm, determined by the thickness of the adhesive tape (see Figure 2). The experimentally measured *Q*-factor is approximately 10^4, as reported previously.[9] The substrates of the two mirrors are fused silica and silicon, respectively. The silicon substrate shows good thermal conductivity and easy integration with the temperature control system, which consists of a Peltier heater, a Pt1000 sensor, and a PID controller with a temperature precision of 0.1 °C.

The FP cavity filled with the DNA and dye solution is externally pumped with a 488 nm pulse laser (Continuum, 5 ns OPO pulsed laser, repetition rate = 20 Hz) through the fused silica substrate mirror that has a transmission coefficient of 80% for the pump light. The pump light is focused into the cavity with a diameter of ∼100 μm. The total sample volume injected in the microfluidic channel is 150 nL, while the sample volume participating in the signal generation is only 0.3 nL. The pump intensity is adjusted by an attenuator. Note that in all our experiment, each signal is obtained by one-single-pulse excitation, and the signal is very stable during all our measurement. The laser or fluorescence signal emission from the FP cavity is free-space coupled into a multimode fiber and transmitted into a spectrometer (Horiba, iHR320) for analysis.

RESULTS

Figure 3 presents the laser emission spectrum for 99 bases target and the corresponding single-base-mismatched DNA at different melting temperatures with two external pump intensity of I_{pump} = 64 μJ/mm^2 and I_{pump} = 417 μJ/mm^2, which corresponds to 4.6$I_{\text{th,25}}$ and 30$I_{\text{th,25}}$, respectively, where $I_{\text{th,25}}$ = 14 μJ/mm^2 is the laser threshold at 25 °C. At low temperature, the target and the mismatched DNA shows multimode laser emission peaks. With the increased temperature, the double-strand DNA starts to melt into single-strand DNA gradually with the release of intercalated dye molecules, which corresponds to a decrease of the concentration of the

DOI: 10.1021/acssensors.8b00481
ACS Sens. 2018, 3, 1750–1755

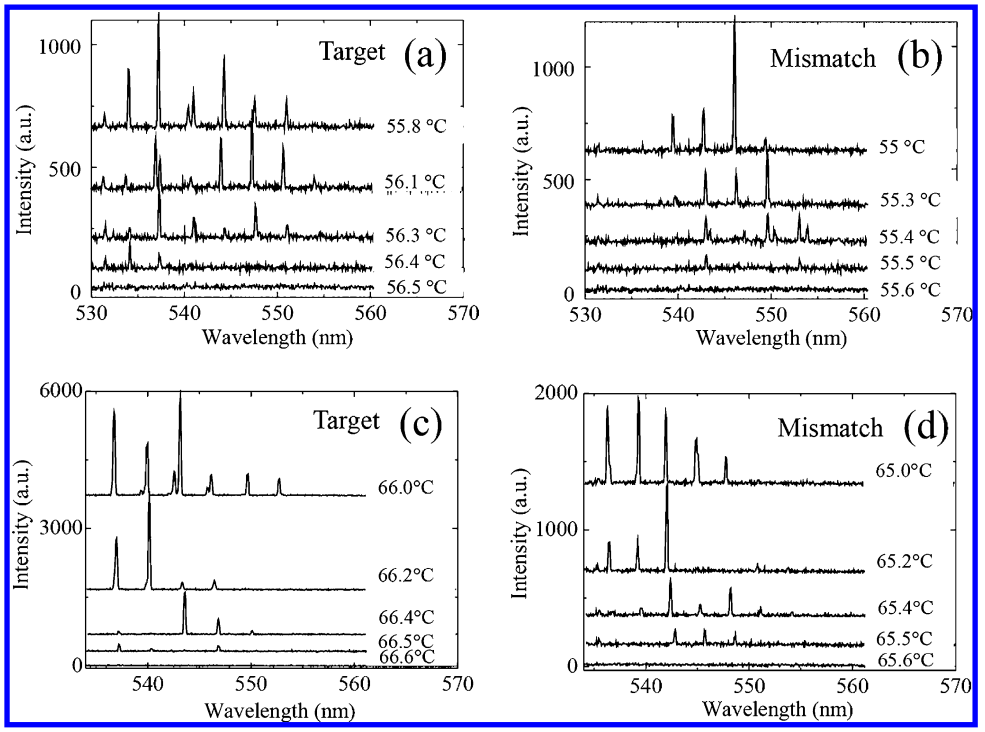

Figure 3. Examples of the laser spectrum for 99 bases target (a, c) and single-base-mismatched (b, d) DNA sequences at excitation pump intensity I_{pump} = 64 μJ/mm^2 = 4.6$I_{th,25}$(a, b) and I_{pump} = 417 μJ/mm^2 = 30$I_{th,25}$ (c, d), where $I_{th,25}$ = 14 μJ/mm^2 is the laser threshold at 25 °C. Curves are vertically shifted for clarity. The DNA sequences are listed in Table S2.

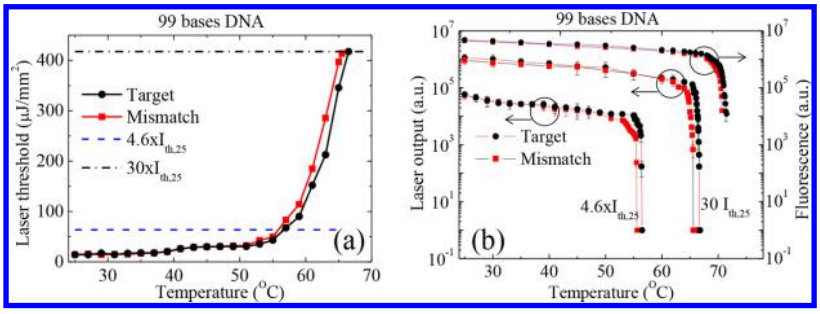

Figure 4. (a) Laser threshold as a function of temperature for 99 bases target and single-base-mismatched DNA sequences. The laser threshold at a given temperature is determined by the linear fit of the lasing-pumping intensity curve at that temperature, as exemplified in Figure 6. (b) Corresponding laser-based HRM curves at two different external pump intensities, I_{pump} = 4.6$I_{th,25}$ (64 μJ/mm^2) and I_{pump} = 30$I_{th,25}$ (417 μJ/mm^2) where $I_{th,25}$ = 14 μJ/mm^2 is the laser threshold at 25 °C. The corresponding fluorescence-based HRM curves are also plotted for comparison. Error bars are obtained with two measurements.

luminescent dyes, i.e., the gain medium. Thus, the laser intensity decreases and eventually disappears, indicating a phase transition from strong laser emission to weak (nearly zero) spontaneous emission (i.e., fluorescence), which can occur within only 0.1 °C temperature change. The difference of the transition temperature for the target and the single-base-mismatched DNA can also be clearly observed. For example, comparison between Figure 3a and b shows that the transition occurs around 56.5 and 55.5 °C, respectively, for the target and the single-base-mismatched DNA sequences. Furthermore, the transition temperature increases by nearly 10 °C when the pump intensity increases from 4.6$I_{th,25}$ to 30$I_{th,25}$.

Figure 4a presents the measured laser threshold as a function of temperature for 99 base target and single-base-mismatched DNA sequences. The threshold shows a rapid increase when the temperature is higher than 55 °C; meanwhile, the threshold difference between the target and the mismatched DNA sequences becomes larger with the increased temperature. Figure 4b shows the corresponding laser output as a function of temperature (i.e., laser-based HRM curve) at different pump intensities (I_{pump} = 4.6$I_{th,25}$ and I_{pump} = 30$I_{th,25}$) as well as the fluorescence-based HRM curves. As shown from the fluorescence curve, the melting temperature, T_m, for the target DNA and the single-base mismatched counterpart is about 70 and 69.3 °C, respectively, with the temperature difference of ΔT_m = 0.7 °C. When pumped with a relatively high pump intensity at I_{pump} = 30$I_{th,25}$, the laser-based melting temperature is 66.6 and 65.6 °C for the target and mismatched DNA sequences, respectively, with the temperature difference of ΔT_m = 1 °C. When the pump intensity is decreased to I_{pump} = 4.6$I_{th,25}$, the melting temperature moves to 56.4 and 55.5 °C for the target and the mismatched DNA sequences, respectively, with the temperature difference of ΔT_m = 0.9 °C. Compared to the fluorescence-based HRM, the melting temperature drops significantly by about 14 °C.

DOI: 10.1021/acssensors.8b00481
ACS Sens. 2018, 3, 1750−1755

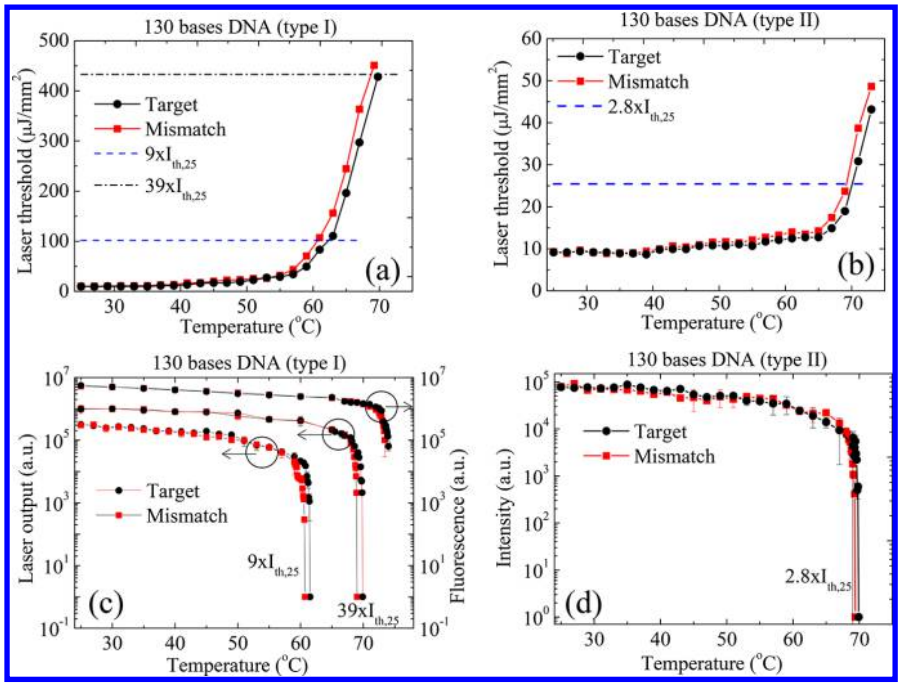

Figure 5. (a,b) Laser threshold as a function of temperature for type I (a) and type II (b) 130 bases target and single-base-mismatched DNA sequences. The laser threshold at a given temperature is determined by the linear fit of the lasing-pumping intensity curve at that temperature, as exemplified in Figure 6. (c,d) Corresponding laser-based HRM curves at different pump intensities. (c) Type I. $I_{pump} = 9I_{th,25}$ (99 μJ/mm^2) and $I_{pump} = 30I_{th,25}$ (330 μJ/mm^2), where $I_{th,25} = 11$ μJ/mm^2 is the laser threshold at 25 °C. The corresponding fluorescence-based HRM curves are also plotted for comparison. (d) Type II. $I_{pump} = 2.8I_{th,25}$, where $I_{th,25} = 9$ μJ/mm^2 is the laser threshold at 25 °C. Note we cannot obtain the corresponding fluorescence-based HRM curves due to the high melting temperature that is close to the solution boiling point. Error bars are obtained by two measurements.

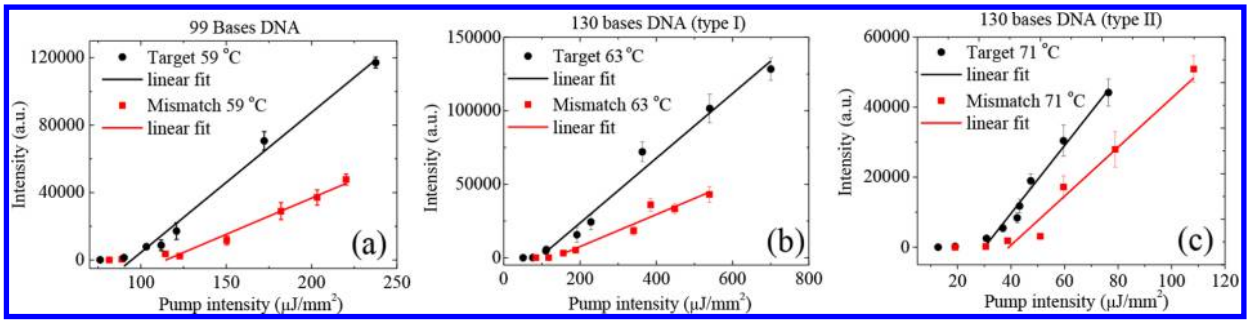

Figure 6. Laser output as a function of pump intensity for 99 bases DNA sequences at 59 °C (a), for type I 130 bases DNA sequences at 63 °C (b) and for type II 130 bases DNA sequences at 71 °C (c). Solid lines are the linear fit above the corresponding laser threshold. Error bars are obtained with three measurements. See also Table S3 for details.

Next, we test the target and single-base-mismatched DNA sequences with longer bases. Figure 5 presents the corresponding experimental results for 130 bases DNA sequences with different GC contents (type I: 21.5%, type II: 48.5%). The laser thresholds at various temperatures are plotted in Figure 5a,b, showing a rapid increase in the threshold with increased temperature. An obvious temperature difference between the target DNA and its mismatched counterpart for a given threshold when the temperature exceeds 57 and 67 °C, respectively, for type I and type II. Figure 5c shows the corresponding laser-based HRM curves for type I at different external pump intensities ($I_{pump} = 9I_{th,25}$ and $I_{pump} = 39I_{th,25}$, where $I_{th,25} = 11$ μJ/mm^2 is the laser threshold at 25 °C) as well as the corresponding fluorescence-based HRM curves. From fluorescence-based HRM curves, we estimate the melting temperature for the target and the mismatched DNA to be around 73 °C, but are unable to clearly distinguish the melting temperature difference due to the 0.1 °C resolution of our temperature control system. In contrast, when pumped at $I_{pump} = 39I_{th,25}$, the laser-based melting temperature is 69.8 and 69.1 °C for the target and the mismatched DNA, respectively, with the temperature difference of $\Delta T_m = 0.7$ °C. When a lower pump intensity is used $I_{pump} = 9I_{th,25}$, the melting temperature is further reduced to 61.4 and 60.6 °C for the target and the mismatched DNA, respectively, with the temperature difference of $\Delta T_m = 0.8$ °C. In this case, the melting temperature drops about 12 °C, compared to the fluorescence-based HRM. For type II DNA sequences, the laser-based melting temperature moves to approximately 70 °C due to higher affinity than their type I counterparts (see Figure 5d). When pumped at $I_{pump} = 2.8I_{th,25}$, where $I_{th,25} = 9$ μJ/mm^2 is the laser threshold at 25 °C, the melting temperature for the target and the single-base-mismatched DNA is 69.9 and 69.4 °C, respectively, with the

DOI: 10.1021/acssensors.8b00481
ACS Sens. 2018, 3, 1750−1755

temperature difference ΔT_m = 0.5 °C. Note that we are unable to obtain the corresponding fluorescence-based HRM curves for type II due to the high melting temperature that is close to the solution boiling point.

Laser-based detection can also provide another method for rapid DNA screening. As shown in Figures 4a and 5a,b, the target and the single-base mismatched DNA sequences can also be differentiated by scanning the pump intensity while keeping the temperature constant. Figure 6 presents the laser output as a function of the pump intensity for 99 bases DNA when the temperature is fixed at 59 °C, for type I 130 bases DNA when the temperature is fixed at 63 °C, and for type II 130 bases DNA when the temperature is fixed at 71 °C. The 99 bases (type I 130 bases, type II 130 bases) target DNA has a laser threshold of 90 $\mu J/mm^2$ (116 $\mu J/mm^2$, 30 $\mu J/mm^2$) and a laser efficiency of 831/($\mu J/mm^2$) (200/($\mu J/mm^2$), 968/($\mu J/mm^2$)), whereas its mismatched counterpart has a higher laser threshold of 114 $\mu J/mm^2$ (156 $\mu J/mm^2$, 38 $\mu J/mm^2$) and a smaller laser efficiency of 430/($\mu J/mm^2$) (109/($\mu J/mm^2$), 698/($\mu J/mm^2$)). The respective ratios are given in Table S3. Note that in the experiment the laser signal is obtained by one single pulse excitation, which can be scanned rapidly and accurately. Therefore, the target and single-base mismatched DNA can be clearly distinguished by the difference in their laser threshold curves such as the threshold and the slope (i.e., laser efficiency). In particular, for type II 130 DNA sequence that has a GC content of 48.5%, the laser slope has a difference as large as 40% (see Table S3) between the target and the single-base mismatched DNA sequences (see Figure 5d), despite the small melting temperature difference of only 0.5 °C.

CONCLUSION

In conclusion, we have demonstrated laser-based DNA melting analysis utilizing the optofluidic lasers based on FP cavities on chip for long DNA sequences. We have first analyzed the method based on the laser theory, and then experimentally investigated the DNA sequences of 99 bases and 130 bases. We first experimentally investigated the dependence of the laser threshold on the temperature and then performed laser-based HRM at different external excitation intensity. Experimental results indicate that the temperature difference between the target and its mismatched counterpart is 0.9 to 1 °C for 99 base DNA sequences and is 0.7−0.8 °C for type I 130 base DNA and about 0.5 °C for type II 130 base DNA. Moreover, the transition temperature of the DNA sequences can be adjusted by choosing a proper excitation intensity, which can be decreased by more than 10 °C, compared to that of the fluorescence-based HRM, especially for those long DNA sequences. Furthermore, an isothermal rapid excitation scanning method has also been developed to differentiate the target and the single-base mismatched DNA samples with long sequences. Our work will lead to novel optofluidic devices that enable rapid and simple analysis of DNAs.

ASSOCIATED CONTENT

Supporting Information

The Supporting Information is available free of charge on the ACS Publications website at DOI: 10.1021/acssensors.8b00481.

Detailed parameters used in the theoretical calculation of Figure 1 in the main text, detailed data extracted from Figure 1 and Figure 6 in the main text, DNA sequence information, and theoretically calculated information for laser-based HRM with different Q values (PDF)

AUTHOR INFORMATION

Corresponding Authors

*E-mail: wangwenjie@tyut.edu.cn.
*E-mail: xsfan@umich.edu.

ORCID

Shaoding Liu: 0000-0003-4809-9815
Xudong Fan: 0000-0003-0149-1326

Author Contributions

§M. H. and X. L. contributed equally to this work.

Notes

The authors declare no competing financial interest.

ACKNOWLEDGMENTS

This work was supported by the National Science Foundation of China (Grant No. 61471254, 61501317, 11574228 and 11304219), Natural Science Foundation of Shanxi Province (Grant No. 201601D011010).

REFERENCES

(1) Wittwer, C. T. High-Resolution Genotyping by Amplicon Melting Analysis Using LCGreen. *Clin. Chem.* **2003**, *49* (6), 853−860.
(2) Liew, M.; Pryor, R.; Palais, R.; Meadows, C.; Erali, M.; Lyon, E.; Wittwer, C. Genotyping of single-nucleotide polymorphisms by high-resolution melting of small amplicons. *Clin. Chem.* **2004**, *50* (7), 1156−1164.
(3) Herrmann, M. G.; Durtschi, J. D.; Bromley, L. K.; Wittwer, C. T.; Voelkerding, K. V. Amplicon DNA melting analysis for mutation scanning and genotyping: cross-platform comparison of instruments and dyes. *Clin. Chem.* **2006**, *52* (3), 494−503.
(4) Reed, G. H.; Kent, J. O.; Wittwer, C. T. High-resolution DNA melting analysis for simple and efficient molecular diagnostics. *Pharmacogenomics* **2007**, *8* (6), 597−608.
(5) Rodriguez Lopez, C. M.; Guzman Asenjo, B.; Lloyd, A. J.; Wilkinson, M. J. Direct detection and quantification of methylation in nucleic acid sequences using high-resolution melting analysis. *Anal. Chem.* **2010**, *82* (21), 9100−9108.
(6) Erali, M.; Wittwer, C. T. High resolution melting analysis for gene scanning. *Methods* **2010**, *50* (4), 250−261.
(7) Lee, W.; Fan, X. Intracavity DNA melting analysis with optofluidic lasers. *Anal. Chem.* **2012**, *84* (21), 9558−9563.
(8) Sun, Y.; Fan, X. Distinguishing DNA by analog-to-digital-like conversion by using optofluidic lasers. *Angew. Chem., Int. Ed.* **2012**, *51* (5), 1236−1239.
(9) Wang, W.; Zhou, C.; Zhang, T.; Chen, J.; Liu, S.; Fan, X. Optofluidic laser array based on stable high-Q Fabry-Perot microcavities. *Lab Chip* **2015**, *15* (19), 3862−3869.

DOI: 10.1021/acssensors.8b00481
ACS Sens. 2018, 3, 1750−1755